

Rapid communication

High-dynamic-range characterization of ultrashort pulses

I.D. Jung, F.X. Kärtner, J. Henkmann, G. Zhang, U. Keller

Ultrafast Laser Physics, Institute of Quantum Electronics, Swiss Federal Institute of Technology, ETH Hönggerberg – HPT, CH-8093 Zürich, Switzerland
(E-mail: jung@iqe.ethz.ch; WWW: http://iqe.ethz.ch/ultrafast/)

Received: 20 June 1997

Abstract. We characterize the quality of ultrashort pulses with pulse widths between 13 and 25 fs by measuring the high-dynamic-range autocorrelations. The pulses were generated from Kerr-lens-modelocked and soliton-modelocked lasers by using broadband semiconductor saturable absorber mirrors. Despite the different modelocking mechanisms, we find comparable performance. The origin of the pulse pedestals can be found from comparisons with numerical simulations.

PACS: 42.55R; 42.60F

The shortest pulses obtained directly from a laser, with pulse widths below 10 fs, are generated by Kerr-lens modelocked (KLM) Ti:sapphire lasers [1–3]. In these lasers, KLM has proven to be an excellent modelocking mechanism [4–7], which is based on the generation of an artificial fast saturable absorber. However, pure KLM pulses in the 10-fs regime are typically not self-starting. Recently, we demonstrated that modelocking of a Ti:sapphire laser in the 10-fs pulse regime is also possible by soliton modelocking, stabilized by a broadband semiconductor saturable absorber mirror (SESAM) [8, 9]. So far, we have achieved self-starting 13-fs pulses. In contrast to KLM, soliton modelocking is based on a slow saturable absorber. The broadband SESAM is a slow saturable absorber because it shows a recovery time of only 60 fs, which is more than four times longer than the pulse width. One expects that the temporal behavior of the saturable absorber has consequences on the pulse quality, which should result in the presence of pulse pedestals. Therefore, larger pedestals are expected for a soliton-modelocked pulse. However, we find similar pulse pedestals in both KLM pulses and soliton-modelocked pulses, when we compare their high-dynamic-range (HDR) autocorrelation measurements. The origin of the measured pulse pedestals can be explained by numerical simulations of the soliton-modelocked laser. We find that not only higher-order dispersion, as shown earlier [10], but also overdriven self-phase modulation (SPM) and bandwidth limitations produce pulse pedestals. When these parameters are varied in the simulations, the resulting pulse

pedestals show the same behavior as those from in the experimental autocorrelations.

In our experiments, we used a Ti:sapphire laser as described in [9] with prism pairs, which provide negative group-delay dispersion (GDD). According to modelocking theory [11], the pulse width τ_p of modelocked lasers with strong soliton formation approaches

$$\tau_p = \frac{4|D|}{\delta W}, \quad (1)$$

where D is the negative GDD, δ the self-phase modulation coefficient, and W the soliton energy. The pulse widths in the KLM and soliton-modelocked lasers are varied from 13 fs to 25 fs by changing the prism insertion. The wavelength dependent GDD of the prism pair causes higher-order dispersion to be also present. We used the KLM laser set-up for the soliton-modelocked laser by replacing only one of the standard dielectric mirrors by a broadband SESAM. Both lasers generate pulses at a constant intracavity pulse energy of 60 nJ, at a center wavelength of 840 nm and at a constant SPM coefficient of approximately (0.2–0.4)/MW. The bandwidth limitations are fixed and given by the gain, the laser optics, the SESAM in the soliton-modelocked laser, and a knife edge in the KLM laser. The knife edge keeps the center wavelength at 840 nm so that both lasers operate at the same wavelength. The HDR autocorrelations were measured as described in [12] but with the difference that we used only reflective optics and a wedged BBO crystal (1 mm to 100 μ m). The time resolution of the HDR set-up is limited to about 16 fs because of the noncollinear geometry. Figures 1a and 1b show, respectively, the measured HDR traces of five KLM and five soliton-modelocked pulses. In both figures, pulse pedestals are present, which grow with decreasing pulse width. For the shortest pulses, the pedestals appear between 10^{-4} and 10^{-3} of the normalized maximum signal. If we try to go even further in decreasing the pulse width, the pulses become unstable. Comparison of both HDR sequences does not show any significant difference, although the modelocking mechanisms are different.

To explain the pulse pedestals we simulated the soliton-modelocked laser. The simulations require knowledge of the

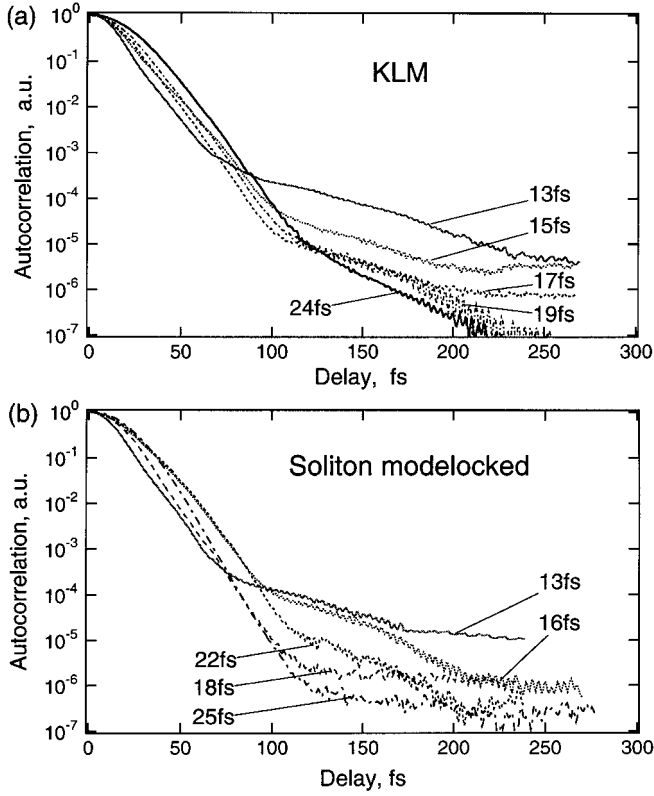


Fig. 1a,b. Measured high-dynamic-range autocorrelations of a pulse sequence with a pulse width of 13 to 25 fs: **a** from a Kerr-lens modelocked laser, **b** from a soliton modelocked laser

time response, the saturation intensity, and the modulation depth of the saturable absorber, which we do not know in the case of the KLM laser. Furthermore, SPM and saturable absorption are coupled in KLM lasers, which result in complex spatio-temporal laser dynamics [13]. Therefore, we did not simulate the KLM laser. The absorber parameters of the SESAM have been independently characterized by pump-probe and saturation-energy measurements, which are described in more detail in [14]. In addition, we incorporated the gain, the loss, the reflectivity of all laser optics, the full dispersion of the prism pair, and the SPM in our numerical

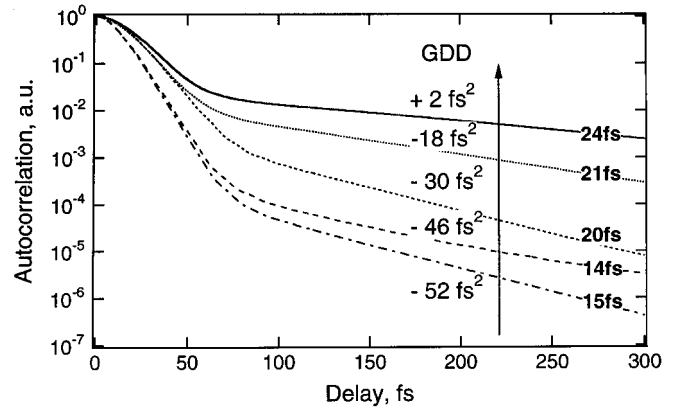


Fig. 2. Calculated high-dynamic-range autocorrelations of a pulse sequence with decreasing negative GDD at a nominal wavelength of 760 nm by moving one of the prisms into the beam. The prism to prism separation is 38 cm

simulations. We used the split-step Fourier transform method to simulate the laser dynamics.

As in the experiments, we reduced the negative GDD by increasing the prism insertion in the numerical simulations. All other parameters were kept constant. However, we started with pulse widths as low as 15 fs to study the transition to instability. We obtained a pulse sequence of auto-correlation traces as shown in Fig. 2. One can see that pulse pedestals grow with decreasing negative GDD. The pulse is shortest when the GDD reaches a nominal value of -46 fs^2 at a wavelength of 780 nm. The pulse width increases again with a further reduction in the negative GDD. To explain this behavior, we show the pulse spectra of this pulse sequence, the net gain profile, and the net GDD of the laser in Fig. 3. With a decreasing negative GDD, the pulse shifts to shorter wavelengths, the width of the pulse spectrum decreases, and a secondary peak grows on the longer wavelength side. With an increasing pulse spectrum, the pulse experiences higher-order dispersion, which destabilizes the pulse. Therefore the pulse shifts to shorter wavelengths, where more negative second-order dispersion is available. The higher negative second order dispersion at shorter wavelengths and the approach to the net gain window force the pulse to become longer. As the pulse shifts to shorter wavelengths, an additional spectral compo-

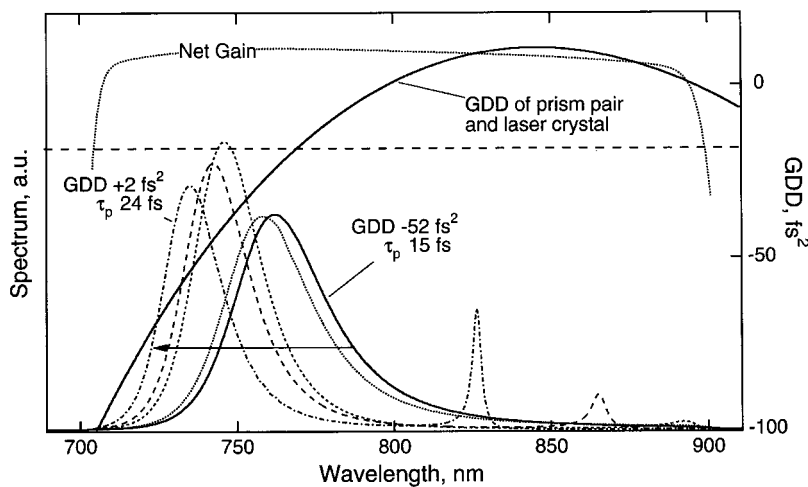


Fig. 3. Calculated pulse spectra for the pulse sequence shown in Fig. 2, with decreasing negative GDD at a nominal wavelength of 760 nm. Also the net gain of the laser is shown. On the right-hand axis, the net GDD of the laser introduced by the prism pair and laser crystal is shown

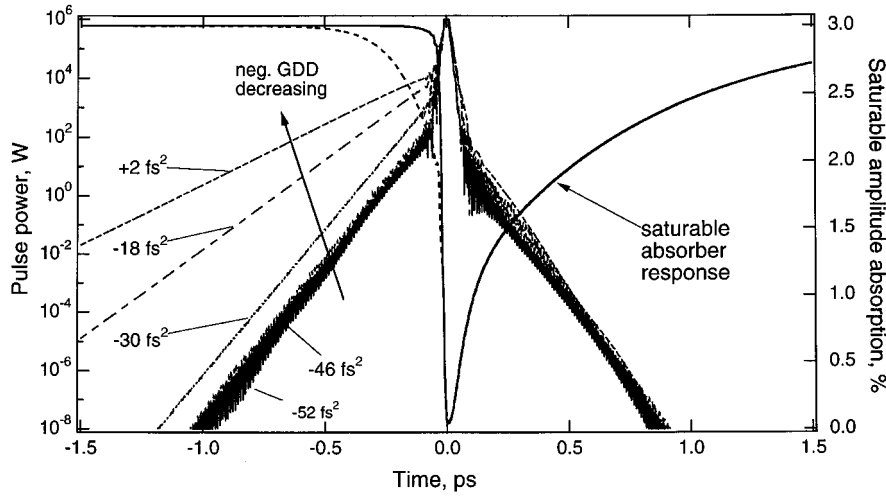


Fig. 4. The calculated pulse power versus time is shown on the left-hand logarithmic axis for a pulse sequence with decreasing negative GDD. The right-hand axis shows the saturable absorber response for the cases -52 fs^2 and $+2 \text{ fs}^2$

ment occurs at longer wavelengths where the dispersion becomes positive. This is due to the phase matching between the soliton and the background pulse, first discussed in [15]. It turns out that this sideband is a forerunner pulse due to the positive dispersion. This can be seen in Fig. 4, which shows a logarithmic plot of the pulse power versus time for the pulse sequence with decreasing negative GDD. Furthermore, the saturable absorber response is plotted with respect to the right-hand axis. The pulses saturate the absorber, which then recovers on a time scale that is much longer than the pulse itself. Stable pulses can still be obtained, because the pulse shaping is done by soliton formation, whereas the absorber only starts and stabilizes the pulse [8]. Therefore, we call this mechanism soliton modelocking. At a GDD value of $+2 \text{ fs}^2$, the energy of the forerunner pulse is so large that it can even appreciably saturate the absorber.

The shortest pulse we achieved in the simulations is 14 fs, which is close to the 13 fs obtained in the experiments. Also, the behavior of the pulse pedestals, shown in Fig. 1 and Fig. 2, is comparable even quantitatively. One could conclude that higher order dispersion is the main cause for the pulse pedestals. However, in the simulations, we used only the smallest SPM value of 0.2 MW and no additional intracavity filter. The knife edge used in the KLM experiments acts

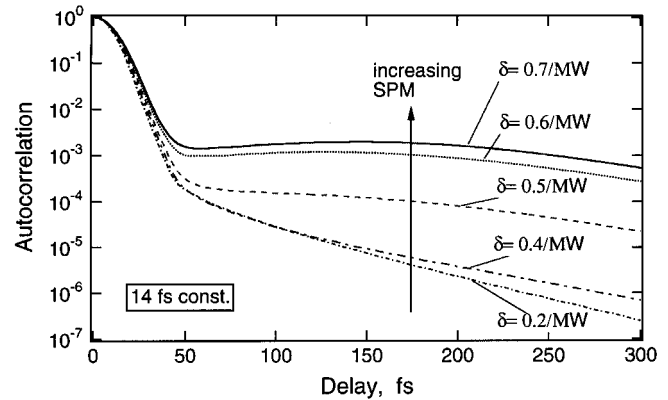


Fig. 5. Calculated high-dynamic-range autocorrelations of a pulse sequence with increasing nonlinear SPM coefficient δ . The pulse width is kept constant at 14 fs by adapting the negative GDD according to (1). Higher-order dispersion is switched off

as a filter, which keeps the center wavelength of the pulse at 840 nm. Also in the soliton-modelocked experiments a filter is present because of the wavelength-dependent losses of the SESAM, which have not been modeled so far. Therefore, it is instructive to investigate the influence of increasing SPM

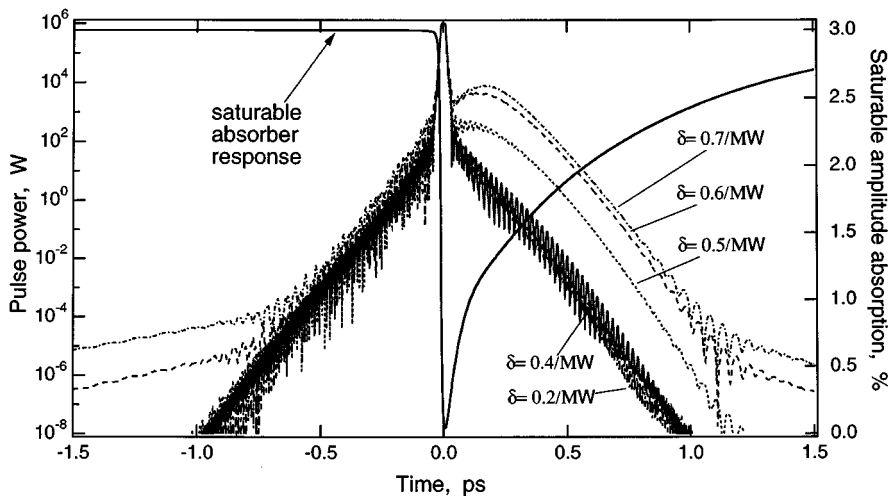


Fig. 6. Calculated pulse power versus time for the pulse sequence shown in Fig. 5 on a logarithmic scale. The saturable absorber response is shown on the right-hand axis

and of an additional intracavity filter. On the growth of pulse pedestals.

First, we investigated the influence of an increasing SPM. We switched off higher-order dispersion and simply adapted D according to (1), in order to maintain the 14 fs, while varying the SPM coefficient from 0.2 to 0.7 MW. Note that only higher-order dispersion contributes to pulse pedestals and not the second-order dispersion D . Figure 5 shows an increase in the pulse pedestal of the simulated autocorrelations with increasing SPM. The corresponding power of the pulse sequence and the absorber response are shown in Fig. 6. The contributions from SPM and GDD, which occur separately in the laser, increased to a level at which the discrete action of SPM cannot be perfectly balanced by the discrete action of the GDD. Therefore, the average soliton experiences additional losses with increasing SPM. This results in a long background pulse, which does not experience the SPM, but only the GDD, and grows preferentially in the open net gain window, gaining energy from the soliton. The pedestal can be understood as a long pulse that is in competition with the soliton for the available gain. Therefore, in steady state, the long pulse is always present. Its energy is determined not only by the gain and loss experienced in the laser, but also by the difference in the net gain between the soliton and the background. Figure 7 shows the pulse spectra of this pulse sequence. In the most overdriven situations, a peak in the spectrum occurs as a result of the long background pulse. This background pulse is called the continuum in soliton perturbation theory. If SPM is overdriven even further, the pulse breaks up into multiple pulses because a regime is entered where the background or continuum experiences more gain in one roundtrip than the single pulse solution.

Second, additional losses of the soliton can also be caused by a filter, as mentioned earlier. Therefore, we find that the influence of an additional intracavity filter also contributes to the growth of pulse pedestals. The SPM coefficient is kept constant here and the dispersion D is adapted according to (1), in order to decrease the pulse width. As in the previous case, a long background pulse grows in the open gain window with decreasing pulse width, because the background does not require as much bandwidth as the solitonlike pulse and, therefore, does not experience the additional bandwidth lim-

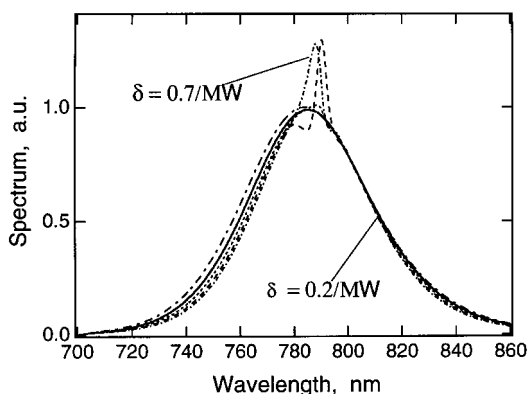


Fig. 7. Calculated pulse spectra for the pulse sequence shown in Fig. 5 with increasing nonlinear SPM coefficient δ

itation as much. Energy is transferred from the soliton to the long pulse. We also find pedestals here, which even exceed a level of 10^{-3} in the HDR autocorrelation for the shortest pulse. In total, the simulations have shown that higher-order dispersion, overdriven SPM, and additional filters cause pulse pedestals. They are all present in our soliton-modelocked laser for the shortest pulses achieved so far. Therefore, it is not possible to isolate them in the experiments. In all simulations, we observe that the pulse pedestals appear up to a level of 10^{-3} to 10^{-4} before they break up into multiple pulsing, which is indicated by the appearance of additional spectral components in the optical spectrum. The same behavior is found in the experiments, where we cannot obtain stable pulses above a pedestal of 10^{-3} of the normalized HDR autocorrelation signal.

In conclusion, we measured pulse pedestals in high-dynamic range autocorrelations of pulses between 13 and 25 fs from prism-controlled, soliton-modelocked and Kerr-lens-modelocked lasers. We find comparable performances despite the difference in the saturable absorber action. Based on numerical simulations of the soliton-modelocked laser, we find that these pulse pedestals appear when the soliton experiences additional losses resulting from the perturbation on the ideal soliton dynamic. Such a loss can be due to higher-order dispersion, overdriven self-phase modulation, or a finite gain bandwidth. The approach of the pulse pedestals to a value of 10^{-3} of the normalized HDR autocorrelation signal is a quantitative criteria for the stability of the pulses and, thus, for the pulse quality.

References

1. I.D. Jung, F.X. Kärtner, N. Matuschek, D.H. Sutter, F. Morier-Genoud, G. Zhang, U. Keller, V. Scheuer, M. Tilsch, T. Tschudi: *Optics Lett.* **22**, 1009 (1997)
2. L. Xu, C. Spielmann, F. Krausz, R. Szepőcs: *Optics Lett.* **21**, 1259 (1996)
3. J. Zhou, G. Taft, C.-P. Huang, M.M. Murnane, H.C. Kapteyn, I.P. Christov: *Optics Lett.* **19**, 1149 (1994)
4. D.E. Spence, P.N. Kean, W. Sibbett: *Optics Lett.* **16**, 42 (1991)
5. U. Keller, G.W. 'tHooft, W.H. Knox, J.E. Cunningham: *Optics Lett.* **16**, 1022 (1991)
6. F. Salin, J. Squier, M. Piché: *Optics Lett.* **16**, 1674 (1991)
7. D.K. Negus, L. Spinelli, N. Goldblatt, G. Feugnet: In *Advanced Solid-State Lasers* Vol. **10**, ed. by G. Dubé, L. Chase (Optical Society of America, Washington DC, 1991) p. 120
8. F.X. Kärtner, I.D. Jung, U. Keller: *Special issue on Ultrafast Electronics, Photonics and Optoelectronics, IEEE J. Selected Topics in Quantum Electronics (JSTQE)* **2**, 540 (1996)
9. R. Fluck, I.D. Jung, G. Zhang, F.X. Kärtner, U. Keller: *Optics Lett.* **21**, 743 (1996)
10. T. Brabec, C. Spielmann, F. Krausz: *Optics Lett.* **17**, 748 (1992)
11. H.A. Haus, J.G. Fujimoto, E.P. Ippen: *JOSA B* **8**, 2068 (1991)
12. A. Braun, J.V. Rudd, S. Cheng, G. Morou, D. Kopf, I.D. Jung, K.J. Weingarten, U. Keller: *Optics Lett.* **20**, 1889 (1995)
13. I.P. Christov, H.C. Kapteyn, M.M. Murnane, C.P. Huang, J. Zhou: *Optics Lett.* **20**, 309 (1995)
14. I.D. Jung, F.X. Kärtner, N. Matuschek, F. Morier-Genoud, Z. Shi, V. Scheuer, M. Tilsch, T. Tschudi, U. Keller: *Appl. Phys. B* **65**, 137 (1997)
15. P.F. Curley, C. Spielmann, T. Brabec, F. Krausz, E. Wintner, A.J. Schmidt: *Optics Lett.* **18**, 54 (1993)